Journal of Magnetic Resonance 297 (2018) 33–41

Contents lists available at ScienceDirect

Journal of Magnetic Resonance

journal homepage: www.elsevier.com/locate/jmr

Chemical shift reference scale for Li solid state NMR derived by first-principles DFT calculations

S.S. Köcher [a,b,c,*], P.P.M. Schleker [b,d], M.F. Graf [b,c], R.-A. Eichel [b,e], K. Reuter [a], J. Granwehr [b,c], Ch. Scheurer [a]

[a] Chair for Theoretical Chemistry and Catalysis Research Center, Technische Universität München, Lichtenbergstraße 4, 85747 Garching, Germany
[b] Institute of Energy and Climate Research (IEK-9), Forschungszentrum Jülich, 52425 Jülich, Germany
[c] Institute of Technical and Macromolecular Chemistry, RWTH Aachen University, Worringerweg 1-2, 52074 Aachen, Germany
[d] Max Planck Institute for Chemical Energy Conversion, Stiftstraße 34-36, 45470 Mülheim an der Ruhr, Germany
[e] Institute of Physical Chemistry, RWTH Aachen University, Landoltweg 2, 52056 Aachen, Germany

ARTICLE INFO

Article history:
Received 6 August 2018
Revised 28 September 2018
Accepted 2 October 2018
Available online 9 October 2018

Keywords:
Solid–state NMR
Lithium NMR
DFT simulations
Chemical shift
Disordered materials
Ionic dynamics

ABSTRACT

For studying electrode and electrolyte materials for lithium ion batteries, solid-state (SS) nuclear magnetic resonance (NMR) of lithium moves into focus of current research. Theoretical simulations of magnetic resonance parameters facilitate the analysis and interpretation of experimental Li SS–NMR spectra and provide unique insight into physical and chemical processes that are determining the spectral profile. In the present paper, the accuracy and reliability of the theoretical simulation methods of Li chemical shielding values is benchmarked by establishing a reference scale for Li SS–NMR of diamagnetic compounds. The impact of geometry, ionic mobility and relativity are discussed. Eventually, the simulation methods are applied to the more complex lithium titanate spinel ($Li_4Ti_5O_{12}$, LTO), which is a widely discussed battery anode material. Simulation of the Li SS–NMR spectrum shows that the commonly adopted approach of assigning the resonances to individual crystallographic sites is not unambiguous.

1. Introduction

Theoretical simulations of chemical shielding are known to support and facilitate the interpretation of experimental nuclear magnetic resonance (NMR) spectra [1]. Theoretical assistance is especially valuable for nuclei for which no extensive empirical correlation schemes are available, such as ^{17}O, ^{31}P, ^{23}Na, ^{27}Al, ^{29}Si or transition metals [2–6]. The theoretical calculation of chemical shielding was initially developed for finite molecules based on a perturbative extension of wave function methods [7–9]. The introduction of the gauge-including projector augmented-wave (GIPAW) [10,11] method in the framework of density functional theory (DFT) also permitted the calculation of nuclear magnetic properties with plane-waves in periodic boundary conditions and thereby also enabled the treatment of extended solid systems.

Solid-state (SS) NMR of lithium is of particular interest for the investigation of materials used for Li ion batteries [12–15]. The structure and Li ion dynamics of electrode as well as electrolyte materials have been investigated extensively. Furthermore, some of the diamagnetic Li compounds that have been studied are of relevance for the formation of a solid–electrolyte interphase (SEI) in conventional batteries as well as for chemical decomposition of solid electrolyte materials [13,16–19]. To be suitable for battery applications, a material must be able to transport Li ions, and electrode materials are required to reversibly store and release Li without structural damage to the host material. For crystalline materials, these prerequisites are generally only fulfilled if a material shows a certain degree of disorder, for example caused by defects or by stochastic occupation of certain crystallographic sites. This combination of disorder and mobility considerably complicates the interpretation of NMR spectra, since the assignment of resonances based on simple empirical rules becomes non-trivial [20]. While spectra interpretation could greatly be simplified by the assistance of chemical shielding simulations, such theoretical calculations pose a considerable challenge due to the narrow chemical shift range experienced by Li nuclei in diamagnetic environments [15,21] and the often broad and overlapping peaks yielded even in magic angle spinning (MAS) experiments due to the dipolar and quadrupolar couplings of the Li nuclei (c.f. SI 1).

In this contribution, the accuracy and reliability of $^{6,7}Li$ chemical shielding simulations is benchmarked by establishing a SS–NMR reference scale for Li [5,22,23]. The calculations are conducted with

* Corresponding author at: Chair for Theoretical Chemistry and Catalysis Research Center, Technische Universität München, Lichtenbergstraße 4, 85747 Garching, Germany.
E-mail address: simone.koecher@ch.tum.de (S.S. Köcher).

https://doi.org/10.1016/j.jmr.2018.10.003
1090-7807/

CASTEP [24], a pseudopotential–plane wave code, and WIEN2k [25], an augmented plane wave (APW) code, which both determine the chemical shielding based on the evaluation of induced current densities [10,11,26]. The impact of geometry, ionic mobility and relativistic effects are discussed [1,2,4,27]. The methodology is first tested using simple lithium salts. Then the simulation method is applied to more complex materials showing multiple sites and exchange between them. Eventually, we simulate a qualitative Li NMR spectrum of lithium titanate (LTO), which is a Li-ion battery electrode material. Based on simplified model assumptions, the difficulties arising when studying ion conducting materials using the conventional concept of resonance assignment according to site occupancy are demonstrated.

2. Theory

The theory section first introduces the chemical shielding tensor and related experimental observables. After outlining the essential concepts for the calculation of chemical shielding with CASTEP, the different approaches for relaxation of the crystal structure are defined. The theory and calculations discussed in this part of the work refer to the CASTEP code package [24]. Only when finally discussing the impact of neighbouring heavy atoms, CASTEP is compared to WIEN2k [25].

2.1. Chemical shielding tensor

The anisotropic second-rank chemical shielding tensor $\boldsymbol{\sigma}$ describes the shielding of the addressed nuclei from the external magnetic field by the local electron density [28]. The chemical shielding tensor can be described by the isotropic chemical shielding

$$\sigma_{\mathrm{iso}} = \frac{\sigma_{xx} + \sigma_{yy} + \sigma_{zz}}{3}, \tag{1}$$

with principal values σ_{xx}, σ_{yy} and σ_{zz} of the shielding tensor, and the shielding anisotropy

$$\sigma_{\mathrm{aniso}} = \sigma_{zz} - \frac{\sigma_{xx} + \sigma_{yy}}{2}, \tag{2}$$

which define the tensor magnitude and the deviation of the tensor from spherical symmetry, respectively [29,30]. The chemical shielding is connected to the chemical shift δ_{iso}, usually reported in literature, via the chemical shielding of a reference substance $\sigma_{\mathrm{iso,ref}}$ as

$$\delta_{\mathrm{iso}} = \frac{\sigma_{\mathrm{iso,ref}} - \sigma_{\mathrm{iso}}}{1 - \sigma_{\mathrm{iso,ref}}} \approx \sigma_{\mathrm{iso,ref}} - \sigma_{\mathrm{iso}}. \tag{3}$$

Since the chemical shielding is defined as the frequency ratio of the resonance frequency and the Larmor frequency of the addressed isotope, chemical shielding and shift are independent of the gyromagnetic ratio γ of the different isotopes ^{6}Li and ^{7}Li. Therefore, in the following discussion, ^{6}Li and ^{7}Li are not distinguished.

2.2. Calculation of chemical shielding

Extended crystalline solids can be modeled with either the cluster approximation or periodic boundary conditions (PBC). For periodic solids, the PBC approach is usually preferred, since the accuracy of the cluster approximation depends on the modeling of the surface at the cluster boundary as well as on the cluster size and symmetry, which influence the charge and multipole distribution throughout the cluster. Pseudopotentials increase the efficiency of PBC calculations with plane waves by approximating the electron density in the nuclear region by an effective core potential.

The shielding σ_{iso} is a measure of the local electron density in the vicinity of the nucleus and its interaction with both the nuclear spin and an external magnetic field. Its calculation crucially depends on the electronic structure at the nuclei and therefore on the applied exchange-correlation (xc) functionals and pseudopotentials. To calculate the all-electron magnetic response for chemical shielding with pseudopotentials in PBC, Pickard and Mauri introduced the GIPAW method [10]. The GIPAW formalism reconstructs the electron density in the nuclear region from the pseudo-electron density while ensuring translational invariance [10,31,32].

The set of xc-functionals applied in this work comprises LDA [33], PBE [34,35], PBEsol [36], and PW91 [37,38], and the default pseudopotentials of different CASTEP release versions (CASTEP7 and CASTEP16) are tested (c.f. SI 2.1).

2.3. Geometry optimization

Since the chemical shielding tensor is known to be very sensitive to geometry [2,29], especially for materials containing light atoms (e.g. hydrogen) the structures experimentally determined by X-ray diffraction (XRD) or neutron scattering might not be accurate enough and such structures will in the following be denoted with the acronym **unopt**. As a remedy to this problem, *ab initio* geometry optimizations are often recommended [5,29]. Three different approaches of geometry optimization are assessed in this work:

free optimization: Both the lattice vectors and the atomic positions are optimized at 0 K without any constraints. The xc-functionals are well known to either underestimate (overbinding for xc-functionals LDA [33] and PBEsol [36]) or overestimate (underbinding for xc-functionals PBE [34,35] and PW91 [37,38]) the interatomic bond lengths [39]. The associated change in the unit cell volume can be circumvented by the following approaches.

fixed cell: Only the atomic positions are relaxed while the experimentally determined lattice vectors from the database are fixed.

Volume **rescale**: The fully relaxed unit cell and atomic positions (c.f. **free opt** option above) are linearly rescaled to the original cell volume reported in the crystallographic database [5].

2.4. Neighbouring heavy anions and relativity

Both CASTEP and WIEN2k divide the periodic electron density into a spherical, atom-centered augmentation region (core region) and an interstitial plane-wave region. Analogously, the induced current density, which determines the induced magnetic field and hence the chemical shielding via the Biot-Savart law, is decomposed into a core and an interstitial contribution. WIEN2k incorporates the interaction of the induced current densities of neighbouring core regions with the nuclear region of interest by the pseudocurrent approach [26]. In contrast, the on-site approximation in CASTEP neglects the impact of the neighbouring augmentation currents on the considered nucleus [10,40].

Heavy nuclei with many electrons are known to be subject to relativistic effects, which increase for larger nuclear charge Z and decreasing distance to the nucleus. Therefore, the incorporation of relativistic effects is crucial for studying nuclear properties, such as chemical shielding, for heavy nuclei [41]. But also light atoms in the vicinity of heavy atoms are known to experience relativistic effects induced by the neighbouring heavy atom and mediated by the electron density within the connecting chemical bond, the so called heavy-atom-light-atom (HALA) effect [42–44]. In general, the relativistic effect is decomposed into a scalar relativistic and a spin–orbit coupling (SOC) contribution. The spin-independent, scalar relativistic terms cover the relativistic correction of the kinetic

and the potential energy, whereas the SOC contribution describes the coupling of the electron spin and angular momentum for heavy nuclei and light nuclei next to them.

In CASTEP, the pseudopotentials representing the core electrons include scalar relativistic effects by default [45], but non-relativistic pseudopotentials can also be chosen. WIEN2k describes the core electrons by atomic-like basis functions (APW method), which are described by the spin-compensated Dirac equation including SOC. The tails of the valence electronic wave functions extending into the core region are considered scalar relativistically (without SOC), whereas relativity is entirely neglected in the interstitial (valence) region. The relativistic effects in WIEN2k can also be turned off. The impact of relativistic terms in the perturbation Hamiltonian are entirely neglected in the following discussion (c.f. SI Table 3).

3. Computational details

The crystal structures of the Li compounds are taken either from the Cambridge Structural Database [46], from the Inorganic Crystal Structure Database [47], or directly from the cited references [48–67].

The chemical shielding calculations and geometry optimizations with CASTEP [10,68] are converged with respect to the cut-off energy and the Monkhorst *k*-point grid. Detailed values employed for the calculations are specified in the SI 2.1. The convergence criterion for both the isotropic and the anisotropic chemical shielding of Li is 0.02 ppm. The geometry optimizations are converged with 0.01 eV for the total energy, 0.005 eV/Å for the forces, and 0.1 GPa for the stress (c.f. SI 2.1). The employed settings are listed in the SI 2.2.

The WIEN2k calculations for the Li halides are conducted with the PBE [34,35] xc-functional based on the experimental crystal structure adopted from the databases [46,47]. The chemical shift (chemical shielding difference with respect to solid LiCl) is converged with respect to size of basis set and number of *k*-points with a convergence threshold of 0.2 ppm (c.f. SI 2.2).

4. Experimental details

Lithium salts were purchased from Sigma Aldrich and used without further purification. Substances without crystal water were stored and rotors were packed in a glovebox with Argon atmosphere. All NMR experiments were performed on a Bruker Avance III HD 400 MHz spectrometer with a Bruker 1.3 mm double resonance MAS probe at a ^{7}Li frequency of 155.5 MHz. The spinning frequency was 60 kHz for all experiments. For single pulse 1D experiment on ^{7}Li, excitation $\pi/2$-pulses of 2.0 µs at 20 W with recovery delays of 150 s were used. The number of accumulations was 4. The ^{7}Li MAS NMR spectra were fitted by Gaussian-Lorentzian lineshapes (c.f. SI 2.3).

5. Results and discussion

5.1. Influence of exchange-correlation functional and pseudopotential

In a first step, the performance and accuracy of the theoretical simulation approach is studied. Table 1 summarizes the simulated and experimental isotropic chemical shifts δ_{iso} for the diamagnetic Li compounds included in the benchmarking. δ_{iso} are calculated as a chemical shielding difference with respect to a reference (δ_{iso}(Li) in crystalline LiCl), which reduces systematic errors of the method to relative errors. Fig. 1 shows for some representative compounds that the different xc-functionals introduce only a small variance in δ_{iso} on the order of < 0.1 ppm. The impact of different pseudopotentials is marginally more pronounced with a variance on the order of 0.4 ppm.

The dependency of the anisotropic chemical shielding σ_{aniso} on both xc-functional and pseudopotential is also rather small (≈ 0.2 ppm) (c.f. Fig. 1). The cubic symmetry of the Li positions in the Li halides, in Li_2O, and in Li_2S is reproduced correctly by yielding $\sigma_{aniso} = 0$ ppm, independently of the applied xc-functional and pseudopotential, if the symmetry is taken into account based on the conventional unit cells (c.f. SI 3). However, both δ_{iso} and σ_{aniso} of compounds with Li resonance frequencies at the fringes of the available range, such as Li_3N, Li_3P or LiCp, are in general more sensitive to modifications of the applied method.

Fig. 2 shows a comparison of the δ_{iso} values calculated based on the **unopt** structures with the experimental data [12,13,21,69–75,77,78,81–83] which yields a generally good agreement (c.f. SI Fig. 7). However, some outlier values, which will be discussed in the following, increase the root mean square error (RMSE) of the linear regression to 1.2 ppm. Table 2 summarizes the linear regression parameters, slope m and intercept n, for correlating the calculated chemical shift δ_{iso}^{calc} to the experimental value δ_{iso}^{exp}

$$\delta_{iso}^{exp} = m\delta_{iso}^{calc} + n, \tag{4}$$

with $m \in [0.88, 0.91]$ and $n \in [-0.66\text{ppm}, -0.64\text{ppm}]$, depending on the applied xc-functional. Comparison with the linear regression parameters derived from the CASTEP7 results, $m \in [0.95, 0.97]$ and $n \in [-0.41\text{ppm}, -0.27\text{ppm}]$, shows that the impact of a different pseudopotential on the correlation between experimental and calculated values is much more pronounced than the effect of different xc-functionals.

5.2. Influence of geometry

The anisotropy σ_{aniso} as the figure of merit for the local symmetry of the electron density is mainly sensitive to the crystal structure. However, not only σ_{aniso} but also the isotropic shift δ_{iso} can differ substantially when considering different geometries, such as hydrates versus anhydrates (c.f. SI Fig. 4), different crystal phases, or magnetically inequivalent Li sites (c.f. SI Table 4). All of the Li substances studied here are very hygroscopic. Some are unstable in the presence of trace amounts of water (e.g. $LiPF_6$). Others build stable, stoichiometric hydrates, such as $LiCl{\cdot}H_2O$ and $LiNO_3{\cdot}3H_2O$. The Li chemical shifts δ_{iso} of the anhydrates and the hydrates can differ substantially (up to 1.2 ppm for $LiNO_3$), since the inclusion of lattice water can change the local electronic structure fundamentally (c.f SI Fig. 4).

In order to eliminate uncertainties in the experimental structure determination, *ab initio* structure relaxations are often recommended prior to the chemical shielding calculations. As depicted in Fig. 3, the impact of the **free opt** and **fixed cell** approach on δ_{iso} is rather small ($\leqslant 0.2$ ppm). As demonstrated by Li_3N and LiCp, the **V rescale** approach can yield rather unphysical descriptions of bond lengths and electron distribution, resulting in considerable distortions of the crystal structure (c.f. SI 4). This distortion effect is primarily relevant for compounds with a significant covalent bonding contribution and can be circumvented by geometry optimizations on the hybrid level [85,86], including a certain ratio of Hartee-Fock nonlocal exact exchange, and by applying dispersion corrections [87–90] to take van–der–Waals interactions into account. In general, the **fixed cell** approach is considered to be the most reliable and physically reasonable relaxation approach, as discussed by Harris et al. [1] It prevents volume changes due to xc-specific under- or overbinding but still allows for the relaxation of the atomic positions within the cell, which can be very important when studying structures containing light atoms close to heavy atoms.

Table 1
The calculated (calc.) isotropic chemical shifts δ_{iso}/ppm for the studied set of diamagnetic Li compounds are summarized together with the experimental (exp.) results and the values found in literature (lit.), which are re-referenced to $LiCl_{(s)}$ if necessary (c.f. SI 1). The isotropic chemical shifts δ_{iso} are calculated with CASTEP16 based on the structures adopted from crystallographic databases. The exp. values are determined by fitting the experimental spectra with a superposition of Gaussian-Lorentzian line shapes (c.f. SI 2.3). The isotropic shifts of crystallographically inequivalent positions are given in parentheses with the number of Li nuclei. If available, experimental and literature data of inequivalent positions are included.

Compound	Calc.	Exp. (this work)	Lit.
$LiBO_2$ [50]	1.09		1.40 [69,70]
$LiAlCl_4$ [57]	−0.09		
Li_2CO_3 [51]	0.95		1.16 [69,70], 1.10 [13], 1.43 [71], 1.20 [72], 0.10 [73]
LiCp [63]	−13.99	−12.53	−12.00 [21]
Li_3N [53]	8.30	7.41	8.59 [74]
	((1) 4.74, (2) 10.07)	((1) 5.79, (2) 8.22)[a]	
$LiNO_3$ [52]	−0.63	−0.56	−0.10 [75]
$LiNO_3{\cdot}3H_2O$ [65]	0.57		
Li_3P [76]	6.37		5.80 [73], 4.61 [77]
	((2) 5.33, (1) 8.45)		
Li_3PO_4 [58]	1.42	1.14	1.50 [78]
	((1) 1.24, (2) 1.51)		
$Li_4P_2S_6$ [79]	1.31		
	((1) 1.03, (1) 1.58)		
$LiPF_6$ [59]	−1.32	−2.02	
Li_2O [54]	4.07	3.67	3.90 [13], 4.05 [71], 4.00 [12], 3.80 [80,81]
Li_2O_2 [55]	0.03		1.25 [71], 1.31 [12], 0.70 [80,81]
	((1) −0.50, (1) 0.56)		
LiOH [56]	2.60		1.43 [75], 2.45 [71], 2.30 [12], 2.30 [72]
$LiOH{\cdot}H_2O$ [66]	2.21		1.50 [13], 1.12 [72]
Li_2S [61]	3.79		3.30 [69,70]
Li_2SO_4[60]	0.48		0.50 [75]
	((1) 0.39, (1) 0.58)		
$Li_2SO_4{\cdot}H_2O$ [67]	0.63		0.50 [82]
	((1) 0.29, (1) 0.97)		((1) 0.2, (1) 0.8) [82]
LiF [48]	0.25	−0.30	0.5 [69,70], 0.10 [13], 0.89 [83]
LiCl [49]	0.00	0.00	
$LiCl{\cdot}H_2O$ [64]	0.35		
	((1) 0.31, (1) 0.40)		
LiBr [48]	0.17		−0.68 [69,70], −0.85 [83]
LiI [49]	−0.06	−3.82	−3.44 [69,70], −3.38 [83]
$LiI{\cdot}H_2O$ [84]	1.18		
$LiIO_3$ [62]	0.83		1.00 [75]

[a] Values determined by assuming two static resonances without exchange.

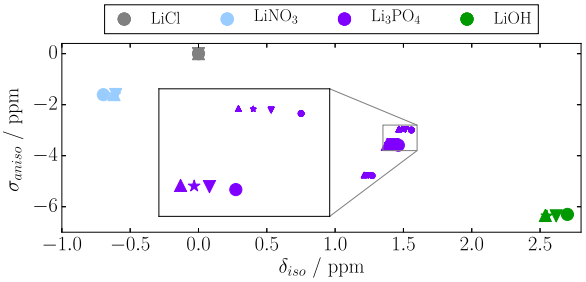

Fig. 1. Isotropic shift δ_{iso} relative to LiCl and the anisotropic σ_{aniso} chemical shielding values calculated with CASTEP16 for some representative Li compounds. The results from calculations with the LDA functional are shown by dots, whereas results based on GGA calculations are depicted by upright triangles (PBE), upside down triangles (PBEsol) and stars (PW91). However, the individual shapes are almost indistinguishable, illustrating the negligible dependency of δ_{iso} and σ_{aniso} on the xc-functional (c.f. inset). For compounds with crystallographically and magnetically inequivalent Li sites (Li_3PO_4. c.f. inset), the individual site-specific chemical shielding is illustrated by smaller symbols, whereas the stoichiometric average is depicted by normal sized symbols.

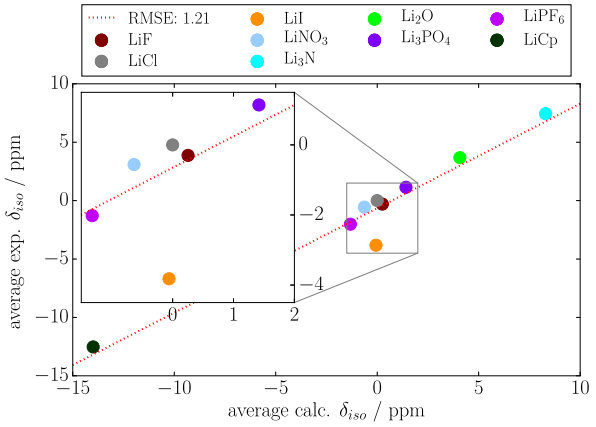

Fig. 2. Correlation of the calculated isotropic chemical shift δ_{iso} (CASTEP16) averaged over the different xc-functionals with experimentally measured ^{7}Li SS–NMR values. The linear regression is depicted by a red dashed line. (For interpretation of the references to colour in this figure legend, the reader is referred to the web version of this article.)

Some of the studied diamagnetic Li compounds have magnetically inequivalent Li sites with different isotropic chemical shifts δ_{iso} (smaller symbols in Fig. 1). For compounds without high ionic conductivity (static Li site occupation), the δ_{iso} differences can in principle be measured experimentally. However, in most cases, the δ_{iso} differences are very small ($\leqslant$ 1.1 ppm) and require the high resolution of ^{6}Li MAS NMR experiments [82,91]. The individual peak positions of the magnetically inequivalent Li sites in $Li_2SO_4{\cdot}H_2O$ reported in [82] are reproduced by calculations with an accuracy of about ±0.2 ppm, whereas the peak difference $\Delta\delta_{iso}$ is in even better agreement with about $<$ ±0.1 ppm.

Table 2
The correlation of the experimentally determined values with the numerically calculated isotropic shifts based on **unopt** structures is analyzed by linear regression. The slope and intercept of the linear regression are determined for calculations with different xc-functionals and pseudopotentials, while the last row provides the xc-average for the different pseudopotentials.

xc	Slope	Intercept	Slope	Intercept
	CASTEP7		CASTEP16	
LDA	0.97	−0.27 ppm	0.88	−0.66 ppm
PBE	0.95	−0.41 ppm	0.90	−0.64 ppm
PW91	0.95	−0.41 ppm	0.91	−0.64 ppm
PBEsol	0.97	−0.35 ppm	0.90	−0.66 ppm
Average	0.96	−0.36 ppm	0.90	−0.65 ppm

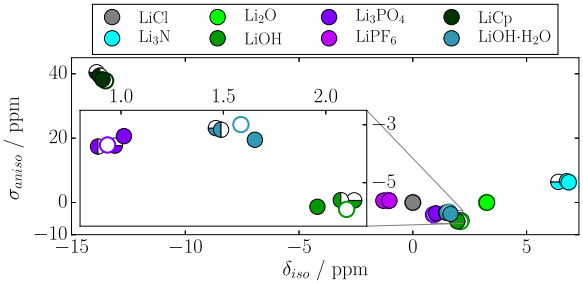

Fig. 3. The isotropic shift δ_{iso} and the anisotropic chemical shielding σ_{aniso} calculated based on the **free opt** (left filled), **V rescale** (bottom filled), and **fixed cell** (empty dots) relaxed structures are compared to the **unopt** (full dots) structures. Since the impact of the different geometry relaxation approaches is rather small, the symbols are almost indistinguishable (c.f. inset). The dots show the average of the CASTEP7 calculations with different xc-functionals for the isotropic shifts and anisotropic shieldings.

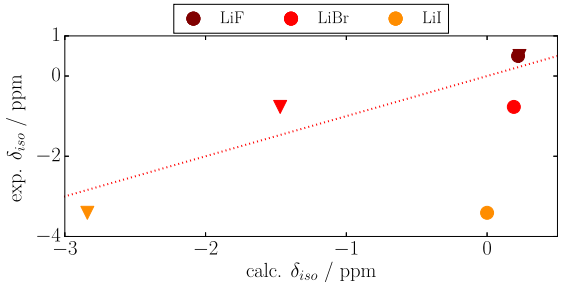

Fig. 4. The Li isotropic chemical shift δ_{iso} of the Li halides simulated with the PBE xc-functional are correlated to experimental Li SS–NMR data from literature. The δ_{iso} calculated with CASTEP16 (dots) and WIEN2k (upside down triangles) are shown based on a scalar relativistic electron density in the core regions. The different halides are marked by different colors and the dotted red line depicts the ideal diagonal correlation ($\delta_{iso}^{calc} = \delta_{iso}^{exp}$). (For interpretation of the references to colour in this figure legend, the reader is referred to the web version of this article.)

The discussion of hydrates and different geometry optimization approaches demonstrates the importance of an accurate crystal structure for the correct calculation of δ_{iso} and σ_{aniso}. The correlation of the calculated δ_{iso} difference of distinguishable, magnetically inequivalent Li sites to experimental data demonstrates the high accuracy of the theoretical calculations and their reliability and versatility for spectra analysis.

5.3. Influence of heavy neighbouring anions

Although the experimental range of Li chemical shifts of diamagnetic compounds in SS–NMR is usually very small [15,21], our correlation studies show a rather consistent and reliable prediction of isotropic Li shifts. Even the compounds at the limits of the available spectrum of resonance frequencies (Li_3N, LiCp) are in good agreement with the linear regression (c.f. Fig. 2). Only LiI represents a significant exception in the correlation of the theoretical results with the experimental data. Since iodine is a very heavy atom and known for its relativistic properties [41–44], it is reasonable to presume relativistic HALA effects as the reason for the discrepancy. However, even calculations in the non-relativistic limit (non-default) show an improved agreement with experiment for WIEN2k calculations in contrast to CASTEP. The default scalar relativistic treatment of the core region in both CASTEP and WIEN2k does not change the Li chemical shift significantly (c.f. SI Table 3). Hence, the superior performance of WIEN2k in comparison to CASTEP for the ionic LiI cannot, at least not as the major contribution, be explained by the covalent relativistic HALA effect (c.f. Fig. 4).

The large atomic number of iodine also implies a large number of electrons, which produce a strong induced current density at the iodine anion. Since CASTEP neglects the interaction between the augmented induced current densities of neighbouring core regions (c.f. Section 2.4), the impact of the iodine current density on the local magnetic field at the Li nucleus is not taken into account. On the other hand, WIEN2k incorporates the induced current density interaction between neighbouring cores by the pseudocurrent approach. The interaction of neighbouring augmented induced current densities increases with heavier nuclei and with decreasing atomic distance. Therefore, this effect is important for LiI, but it is no longer observable in $LiIO_3$, where the oxygen screens the Li nuclei from the core region of the iodine.

Of course, relativistic effects such as the HALA effect are most likely still important to explain the residual discrepancy between calculated and observed chemical shift in LiI. However, the HALA effect mediated by SOC is expected to be not as pronounced as for H-I or C-I bonds, since the Li-I distance is much larger than the H-I and C-I bond lengths. Furthermore, the electron density in the more ionic Li-I bond is significantly reduced in comparison to the covalent HI and CI bonds resulting in a reduced SOC transfer between the nuclei [42].

Summing up, for heavy nuclei with many electrons in the direct neighbourhood to Li, the on-site approximation of CASTEP is not appropriate. Furthermore, relativistic HALA effects can play a role, but are likely less pronounced than in covalent compounds.

5.4. Ion conducting solids

In the ^{7}Li MAS NMR experiments presented in this work, inequivalent Li positions can only be resolved for Li_3N as two partially overlapping peaks of intensity ratio $\approx 1:2$ (c.f. Fig. 5 red). However, Li_3N is known to be a good solid Li-ion conductor, caused by the high intralayer conductivity within the Li-N layer of about 10^{-2} to 0.1 S/m [92,93]. The interlayer conductivity, which is about two to three orders of magnitude smaller, describes the exchange motion of Li between the Li-N layer and the pure Li layer in Li_3N (c.f. SI Fig. 6a) [92–97]. This site exchange motion of the Li ions between the crystallographically inequivalent Li sites causes

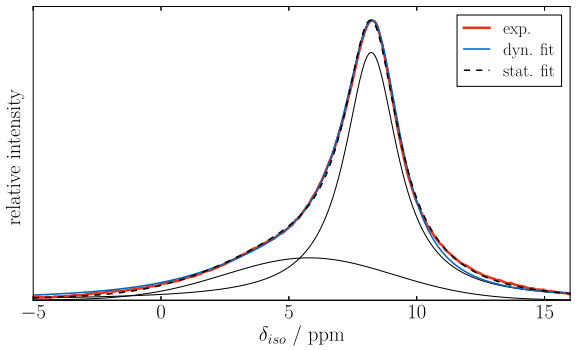

Fig. 5. Li SS–NMR spectrum of Li_3N. The experimental ^7Li spectrum, depicted in red, features two partially overlapping peaks corresponding to the two crystallographically inequivalent positions. The experimental lineshape (red) is fitted by two Lorentz-Gauss peaks (dashed black) neglecting Li exchange. The static fit results in two resonances at 5.79 and 8.22 ppm (solid black). The dynamic fit including Li exchange and based on the chemical shifts determined with CASTEP16 results in an exchange rate of 1776 s^{-1} and is shown in blue. (For interpretation of the references to colour in this figure legend, the reader is referred to the web version of this article.)

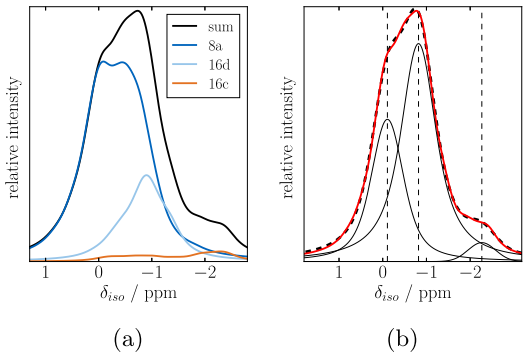

Fig. 6. Simulated Li SS–NMR spectrum of LTO. (a) Contributions of the *8a* (blue), *16d* (light blue) and *16c* (orange) sites to the total simulated spectrum (black). (b) Decomposition of the simulated spectrum (red) using a model consisting of three Voigt resonance lines (solid black). The sum of the three lines (black dashed line) shows a good agreement with the simulated spectrum. The vertical black dashed lines show the chemical shifts at −0.1, −0.8, and −2.3 ppm obtained from the fitted resonance lines. (For interpretation of the references to colour in this figure legend, the reader is referred to the web version of this article.)

further line broadening in addition to the relaxation line broadening and reduction of the peak distance $\Delta\delta_{iso}$, which is supposed to narrow even further with increasing temperature.

In the experimental spectrum in Fig. 5 (red), the simulated isotropic shifts of the individual Li positions (4.74 and 10.07 ppm with CASTEP16) are not visible as two fully resolved peaks. Fitting the MAS NMR spectrum with a superposition of individual lines (c.f. SI 2.3) is not a physically justified approach for exchanging systems, since it only yields effective parameters that provide, at best, a lower limit for the chemical shift difference between the peaks. In order to unambiguously separate the contributions by chemical exchange and relaxation on the spectral lineshape, additional, elaborate NMR measurements at different temperatures and magnetic fields would be required. In contrast, the theoretical simulations provide the chemical shift difference of the crystallographically inequivalent Li nuclei, $\Delta\delta_{iso} = 5.33$ ppm (c.f. Table 1), without prior knowledge of either ionic or relaxation dynamics. By using the numerically calculated $\Delta\delta_{iso}$ and the Li site ratio as the only constraints for fitting the spectrum with a model that includes two-site exchange [98,99], it is possible to obtain an estimate for the exchange rate (1776 s^{-1}) that is well in line with literature values (c.f. SI 2.4) [92,94,100]. Without an estimate for $\Delta\delta_{iso}$, reasonable fits are possible with exchange rates differing by an order of magnitude from literature values.

The solid materials commonly used in batteries are usually structurally more complex than the crystalline compounds studied so far. For example, the diamagnetic lithium-titanium-oxide ($Li_4Ti_5O_{12}$, LTO) crystallizes in a cubic, spinel-like structure with $Fd\bar{3}m$ symmetry. The Li cations mostly occupy tetrahedral *8a*, octahedral *16d*, and *16c* sites, where the octahedral *16d* sites are shared with Ti cations. Due to the occupational disorder in combination with Li mobility, LTO yields rather complex Li MAS NMR spectra, which show a certain dependency on the method of synthesis. The experimental spectra are commonly analyzed by fitting and assigning the individual peaks to the different crystallographic Li positions [91,104,106].

Preliminary simulations of isotropic Li NMR spectra of LTO based on the calculated Li chemical shifts δ_{iso} are shown in Fig. 6a. The simulated spectra qualitatively reproduce the structure and features of the experimental spectra [91,104] fairly well, even though neither a representative sample of the space of possible Li positions, nor the structure-observable relationship or the Li mobility are taken into account (c.f. SI 2.5) [109]. The quantitative differences between the experimental spectra and the simulation

Table 3
Experimental [75,91,101–108] and calculated values of δ_{iso} for Li at the different crystallographic positions in $Li_4Ti_5O_{12}$. The chemical shifts are given with respect to LiCl in aqueous solution.

Li site	*8a*	*16d*	*16c*
δ_{iso}^{calc} / ppm	−1.2 to 0.9	−1.4 to 0.5	−2.5 to 0.8
δ_{iso}^{exp} / ppm	0.3 [103,104], 0.7 [91], 0.1 [75,107], 0.2 [101], 0.0 [102,105,108]	−0.2 [103,104], 0.2 [91], −0.3 [75,107], −0.1 [101], −1.1 [102], 0.0 [105,108]	−0.7 [103,104], −0.5 [91], −0.3 [75,107]

likely arise from the severe approximations. The calculations clearly indicate that for LTO, the approach of assigning resonances to crystallographic sites is not necessarily justified and may actually be misleading. The theoretical simulations summarized in Table 3 show that Li in a particular site cannot be associated with a specific resonance, but that each of the sites adds a multi-line contribution to the spectrum (Fig. 6a). In Fig. 6b a fit of the calculated spectrum with three different resonance lines is shown. The overall fit agrees well with the spectrum, even though the originating contributions to the spectrum are of a different nature. The obtained resonances from this fit are consistent with results reported in literature for fits of experimental spectra, which indicates that distinguishable experimental peaks likely consist of contributions from multiple crystallographic Li sites.

The LTO example demonstrates the benefit and value of theoretical calculations of δ_{iso} in analyzing and interpreting experimental Li NMR spectra. The achieved accuracy of the simulations is sufficient to gain valuable information even for diamagnetic compounds, despite their small frequency range and frequently mediocre resolution of experimental Li NMR spectra due to quadrupolar broadened lines.

6. Conclusion

The GIPAW pseudopotential plane wave method as implemented in CASTEP is applied to a set of diamagnetic Li compounds. The method generally proofs to be accurate enough to reproduce the isotropic chemical shift of Li over the entire available spectral range.

The choice of xc-functional shows only a minor effect on the chemical shift. The linear regression of the correlation between calculated δ_{iso}^{calc} (CASTEP16) and experimental δ_{iso}^{exp} chemical shifts yields slope m and intercept n parameters in the range of $m \in [0.88, 0.91]$ and $n \in [-0.66\text{ppm}, -0.64\text{ppm}]$, depending on the xc-functional. The impact of the applied pseudopotential on the linear correlation parameters is found to be somewhat more distinct and non-negligible. In contrast to the results found for other nuclei [1,5], for the Li compounds studied in this paper, the experimental crystal structures perform well and the improvement achieved by additional geometry relaxation is negligible. Furthermore, for the Li compounds discussed here, no significant impact from including relativistic effects can be identified. LiI is the only observed exception of the generally reliable and good benchmark of the method, since the on-site approximation neglects the induced current density of nearest neighbouring electron-rich ions.

For the application of Li SS–NMR to study Li-ion battery materials, Li ionic mobility and non-periodic disorder in the structures have a substantial impact on the spectral profile and the lineshape. The theoretically simulated Li SS-NMR spectrum of Li_3N is in good agreement with experimental results, allowing us to confirm models about the Li mobility in the material. For LTO, the inclusion of occupational disorder in the simulation demonstrates that each crystallographic site provides a multi-line contribution to the spectrum, which is impossible to resolve without theoretical support. Both the Li_3N and the LTO examples are showcases for the complexity and ambiguity of SS–NMR spectra of Li ion conducting solids.

Acknowledgments

We appreciate stimulating discussions with Matt Probert, Vladimir Malkin, Olga Malkina, Martin Kaupp, and Marc Paulus. We thank Anja Paulus for assistance with XRD measurements and Markus Schuderer for support with CASTEP calculations. The authors gratefully acknowledge the computing time granted through JARA-HPC on the supercomputer JURECA [110] at Forschungszentrum Jülich and by the Leibniz Rechenzentrum der Bayerischen Akademie der Wissenschaften. MFG was supported by the German Federal Ministry of Education and Research (BMBF project DESIREE, grant number 03SF0477A).

Appendix A. Supplementary material

Supplementary data associated with this article can be found, in the online version, at https://doi.org/10.1016/j.jmr.2018.10.003.

References

[1] R.K. Harris, P. Hodgkinson, C.J. Pickard, J.R. Yates, V. Zorin, Chemical shift computations on a crystallographic basis: some reflections and comments, Magn. Reson. Chem. 45 (S1) (2007) S174–S186. http://onlinelibrary.wiley.com/doi/10.1002/mrc.2132/abstract .

[2] T. Charpentier, The PAW/GIPAW approach for computing NMR parameters: a new dimension added to NMR study of solids, Solid State Nucl. Magn. Reson. 40 (1) (2011) 1–20. http://www.sciencedirect.com/science/article/pii/S0926204011000440 .

[3] M. Kaupp, V.G. Malkin, O.L. Malkina, D.R. Salahub, Calculation of ligand NMR chemical shifts in transition-metal complexes using ab initio effective-core potentials and density functional theory, Chem. Phys. Lett. 235 (3–4) (1995) 382–388. http://www.sciencedirect.com/science/article/pii/000926149500108G .

[4] C. Bonhomme, C. Gervais, F. Babonneau, C. Coelho, F. Pourpoint, T. Azaïs, S.E. Ashbrook, J.M. Griffin, J.R. Yates, F. Mauri, C.J. Pickard, First-Principles calculation of NMR parameters using the gauge including projector augmented wave method: a chemist's point of view, Chem. Rev. 112 (11) (2012) 5733–5779.

[5] F. Vasconcelos, S. Cristol, J. Paul, L. Montagne, F. Mauri, L. Delevoye, First-principles calculations of NMR parameters for phosphate materials, Magn. Reson. Chem. 48 (S1) (2010) S142–S150. http://onlinelibrary.wiley.com/doi/10.1002/mrc.2667/abstract .

[6] A.L. Michan, B.S. Parimalam, M. Leskes, R.N. Kerber, T. Yoon, C.P. Grey, B.L. Lucht, Fluoroethylene carbonate and vinylene carbonate reduction: understanding Lithium-Ion battery electrolyte additives and solid electrolyte interphase formation, Chem. Mater. 28 (22) (2016) 8149–8159, https://doi.org/10.1021/acs.chemmater.6b02282.

[7] W. Kutzelnigg, Theory of magnetic susceptibilities and NMR chemical shifts in terms of localized quantities, Isr. J. Chem. 19 (1-4) (1980) 193–200. http://onlinelibrary.wiley.com.eaccess.ub.tum.de/doi/10.1002/ijch.198000020/abstract .

[8] W. Kutzelnigg, U. Fleischer, M. Schindler, The IGLO-Method: ab-initio calculation and interpretation of NMR chemical shifts and magnetic susceptibilities, in: Deuterium and Shift Calculation, NMR Basic Principles and Progress, vol. 23, Springer, Berlin Heidelberg, 1990, pp. 165–263. http://www.springer.com/chemistry/physical+chemistry/book/978-3-642-75934-5 .

[9] J. Gauss, Calculation of NMR chemical shifts at second-order many-body perturbation theory using gauge-including atomic orbitals, Chem. Phys. Lett. 191 (6) (1992) 614–620. http://www.sciencedirect.com/science/article/pii/0009261492855985 .

[10] C.J. Pickard, F. Mauri, All-electron magnetic response with pseudopotentials: NMR chemical shifts, Phys. Rev. B 63 (24) (2001) 245101. http://link.aps.org/doi/10.1103/PhysRevB.63.245101 .

[11] C.J. Pickard, F. Mauri, Nonlocal pseudopotentials and magnetic fields, Phys. Rev. Lett. 91 (19) (2003) 196401. https://link.aps.org/doi/10.1103/PhysRevLett.91.196401 .

[12] Z. Zhu, A. Kushima, Z. Yin, L. Qi, K. Amine, J. Lu, J. Li, Anion-redox nanolithia cathodes for Li-ion batteries, Nat. Energy 1 (2016) 16111. http://www.nature.com/articles/nenergy2016111 .

[13] B.M. Meyer, N. Leifer, S. Sakamoto, S.G. Greenbaum, C.P. Grey, High field multinuclear NMR investigation of the SEI layer in lithium rechargeable batteries, Electrochem. Solid-State Lett. 8 (3) (2005) A145–A148. http://esl.ecsdl.org/content/8/3/A145 .

[14] K. Ogata, E. Salager, C.J. Kerr, A.E. Fraser, C. Ducati, A.J. Morris, S. Hofmann, C.P. Grey, Revealing lithium–silicide phase transformations in nano-structured silicon-based lithium ion batteries via in situ NMR spectroscopy, Nat. Commun. 5 (3217) (2014) 1–11. http://www.nature.com/ncomms/2014/140203/ncomms4217/full/ncomms4217.html .

[15] C.P. Grey, N. Dupré, NMR studies of cathode materials for Lithium-Ion rechargeable batteries, Chem. Rev. 104 (10) (2004) 4493–4512.

[16] Y. Zhu, X. He, Y. Mo, Origin of outstanding stability in the lithium solid electrolyte materials: Insights from thermodynamic analyses based on First-Principles calculations, ACS Appl. Mater. Interf. 7 (42) (2015) 23685–23693.

[17] Y. Zhu, X. He, Y. Mo, First principles study on electrochemical and chemical stability of solid electrolyte–electrode interfaces in all-solid-state Li-ion batteries, J. Mater. Chem. A 4 (9) (2016) 3253–3266. http://pubs.rsc.org/en/content/articlelanding/2016/ta/c5ta08574h .

[18] F. Han, Y. Zhu, X. He, Y. Mo, C. Wang, Electrochemical stability of $Li_{10}GeP_2S_{12}$ and $Li_7La_3Zr_2O_{12}$ solid electrolytes, Adv. Energy Mater. 6 (8) (2016) 1501590. http://onlinelibrary.wiley.com/doi/10.1002/aenm.201501590/abstract .

[19] A.C. Luntz, J. Voss, K. Reuter, Interfacial challenges in solid-state Li ion batteries, J. Phys. Chem. Lett. 6 (22) (2015) 4599–4604, https://doi.org/10.1021/acs.jpclett.5b02352.

[20] M.F. Graf, H. Tempel, S.S. Köcher, R. Schierholz, C. Scheurer, H. Kungl, R. Eichel, J. Granwehr, Observing different modes of mobility in lithium titanate spinel by nuclear magnetic resonance, RSC Adv. 7 (41) (2017) 25276–25284. http://pubs.rsc.org/en/content/articlelanding/2017/ra/c7ra01622k .

[21] C. Elschenbroich, Organometallics, 3rd ed., Wiley-VCH, Weinheim, 2006. http://opac.ub.tum.de/InfoGuideClient.tumsis/start.do?Login=wotum03&Query=540=3-527-29390-6 .

[22] F. Vasconcelos, S. Cristol, J. Paul, G. Tricot, J. Amoureux, L. Montagne, F. Mauri, L. Delevoye, ^{17}O Solid-State NMR and First-Principles calculations of sodium trimetaphosphate ($Na_3P_3O_9$), tripolyphosphate ($Na_5P_3O_{10}$), and pyrophosphate ($Na_4P_2O_7$), Inorg. Chem. 47 (16) (2008) 7327–7337.

[23] I. Alkorta, J. Elguero, Ab initio (GIAO) calculations of absolute nuclear shieldings for representative compounds containing $^{1(2)}H$, $^{6(7)}Li$, ^{11}B, ^{13}C, $^{14(15)}N$, ^{17}O, ^{19}F, ^{29}Si, ^{31}P, ^{33}S, and ^{35}Cl nuclei, Struct. Chem. 9 (3) (1998) 187–202. http://link.springer.com.eaccess.ub.tum.de/article/10.1023/A%3A1022419030317 .

[24] M. Segall, M. Probert, C. Pickard, P. Hasnip, S. Clark, K. Refson, J.R. Yates, M. Payne, P. Lindan, P. Haynes, J. White, V. Milman, N. Govind, M. Gibson, P. Tulip, V. Cocula, B. Montanari, D. Quigley, M. Glover, L. Bernasconi, A. Perlov, M. Plummer, E. McNellis, J. Meyer, J. Gale, D. Jochym, J. Aarons, B. Walker, R. Gillen, D. Jones, T. Green, I.J. Bush, C.J. Armstrong, E.J. Higgins, E.L. Brown, M.S. McFly, CASTEP – Cambridge serial total energy package: Ab initio total energy program, 2016.

[25] P. Blaha, K. Schwarz, G.K.H. Madsen, D. Kvasnicka, J. Luitz, WIEN2k, an augmented plane wave plus local orbitals program for calculating crystal properties, 2016.

[26] R. Laskowski, P. Blaha, Calculations of NMR chemical shifts with APW-based methods, Phys. Rev. B 85 (3) (2012) 035132. http://link.aps.org/doi/10.1103/PhysRevB.85.035132 .

[27] M. Bühl, M. Kaupp, O.L. Malkina, V.G. Malkin, The DFT route to NMR chemical shifts, J. Comput. Chem. 20 (1) (1999) 91–105. http://onlinelibrary.wiley.com/doi/10.1002/(SICI)1096-987X(19990115)20:1<91::AID-JCC10>3.0.CO;2-C/abstract .

[28] M. Kaupp, M. Bühl, V.S. Malkin, Calculation of NMR and EPR Parameters, first ed., Wiley-VCH, Weinheim, 2004. http://opac.ub.tum.de/

InfoGuideClient.tumsis/start.do?Login=wotum03&Query=540=3-527-30779-6 .
[29] R.K. Harris, E.D. Becker, S.M.C. de Menezes, P. Granger, R.E. Hoffman, K.W. Zilm, Further conventions for NMR shielding and chemical shifts (IUPAC recommendations 2008), Pure Appl. Chem. 80 (1) (2008) 59–84. http://pac.iupac.org/publications/pac/80/1/0059/ .
[30] F.A.L. Anet, D.J. O'Leary, The shielding tensor. part I: understanding its symmetry properties, Concepts Magn. Reson. 3 (4) (1991) 193–214.
[31] C.G.V. de Walle, P.E. Blöchl, First-principles calculations of hyperfine parameters, Phys. Rev. B 47 (8) (1993) 4244–4255. http://link.aps.org/doi/10.1103/PhysRevB.47.4244 .
[32] P.E. Blöchl, Projector augmented-wave method, Phys. Rev. B 50 (24) (1994) 17953–17979. http://link.aps.org/doi/10.1103/PhysRevB.50.17953 .
[33] W. Kohn, L.J. Sham, Self-consistent equations including exchange and correlation effects, Phys. Rev. 140 (4A) (1965) A1133–A1138. https://link.aps.org/doi/10.1103/PhysRev.140.A1133 .
[34] J.P. Perdew, K. Burke, M. Ernzerhof, Generalized gradient approximation made simple, Phys. Rev. Lett. 77 (18) (1996) 3865–3868. https://link.aps.org/doi/10.1103/PhysRevLett.77.3865 .
[35] J.P. Perdew, K. Burke, M. Ernzerhof, Generalized gradient approximation made simple [Phys. Rev. Lett. 77, 3865 (1996)], Phys. Rev. Lett. 78 (7) (1997) 1396. https://link.aps.org/doi/10.1103/PhysRevLett.78.1396 .
[36] J.P. Perdew, A. Ruzsinszky, G.I. Csonka, O.A. Vydrov, G.E. Scuseria, L.A. Constantin, X. Zhou, K. Burke, Restoring the density-gradient expansion for exchange in solids and surfaces, Phys. Rev. Lett. 100 (13) (2008) 136406. https://link.aps.org/doi/10.1103/PhysRevLett.100.136406 .
[37] J.P. Perdew, J.A. Chevary, S.H. Vosko, K.A. Jackson, M.R. Pederson, D.J. Singh, C. Fiolhais, Atoms, molecules, solids, and surfaces: applications of the generalized gradient approximation for exchange and correlation, Phys. Rev. B 46 (11) (1992) 6671–6687. https://link.aps.org/doi/10.1103/PhysRevB.46.6671 .
[38] J.P. Perdew, J.A. Chevary, S.H. Vosko, K.A. Jackson, M.R. Pederson, D.J. Singh, C. Fiolhais, Erratum: atoms, molecules, solids, and surfaces: applications of the generalized gradient approximation for exchange and correlation, Phys. Rev. B 48 (7) (1993) 4978. https://link.aps.org/doi/10.1103/PhysRevB.48.4978.2 .
[39] G.I. Csonka, J.P. Perdew, A. Ruzsinszky, P.H.T. Philipsen, S. Lebègue, J. Paier, O. A. Vydrov, J.G. Ángyán, Assessing the performance of recent density functionals for bulk solids, Phys. Rev. B 79 (15) (2009) 155107. https://link.aps.org/doi/10.1103/PhysRevB.79.155107 .
[40] J.R. Yates, C.J. Pickard, M.C. Payne, F. Mauri, Relativistic nuclear magnetic resonance chemical shifts of heavy nuclei with pseudopotentials and the zeroth-order regular approximation, J. Chem. Phys. 118 (13) (2003) 5746–5753. http://aip.scitation.org.eaccess.ub.tum.de/doi/abs/10.1063/1.1541625 .
[41] J. Autschbach, S. Zheng, Chapter 1 relativistic computations of NMR parameters from first principles: Theory and applications, in: G.A. Webb (Ed.), Annual Reports on NMR Spectroscopy, vol. 67, Academic Press, 2009, pp. 1–95. http://www.sciencedirect.com/science/article/pii/S0066410309067015 .
[42] S. Komorovský, M. Repiský, O.L. Malkina, V.G. Malkin, I.M. Ondík, M. Kaupp, A fully relativistic method for calculation of nuclear magnetic shielding tensors with a restricted magnetically balanced basis in the framework of the matrix Dirac–Kohn–Sham equation, J. Chem. Phys. 128 (10) (2008) 104101. http://aip.scitation.org/doi/10.1063/1.2837472 .
[43] M. Kaupp, O.L. Malkin, V.G. Malkin, Interpretation of 13C NMR chemical shifts in halomethyl cations. On the importance of spin-orbit coupling and electron correlation, Chem. Phys. Lett. 265 (1) (1997) 55–59. http://www.sciencedirect.com/science/article/pii/S000926149601425X .
[44] M. Kaupp, O.L. Malkina, V.G. Malkin, P. Pyykkö, How do Spin-Orbit-Induced Heavy-Atom effects on NMR chemical shifts function? validation of a simple analogy to Spin- Spin coupling by density functional theory (DFT) calculations on some iodo compounds 4 (1) (1998) 118–126. <http://www.onlinelibrary.wiley.com/doi/abs/10.1002/%28SICI%291521-3765%28199801%294%3A1%3C118%3A%3AAID-CHEM118%3E3.0.CO%3B2-6>.
[45] D.D. Koelling, B.N. Harmon, A technique for relativistic spin-polarised calculations, J. Phys. C: Solid State Phys. 10 (16) (1977) 3107. http://stacks.iop.org/0022-3719/10/i=16/a=019 .
[46] C.R. Groom, I.J. Bruno, M.P. Lightfoot, S.C. Ward, The Cambridge structural database, Acta Cryst. B B72 (2016) 171–179.
[47] G. Bergerhoff, I.D. Brown, ICSD, FIZ Karlsruhe. https://icsd.fiz-karlsruhe.de/search/index.xhtml (May 2016). <https://icsd.fiz-karlsruhe.de/search/index.xhtml>.
[48] W.P. Davey, Precision measurements of crystals of the alkali halides, Phys. Rev. 21 (2) (1923) 143–161. http://link.aps.org/doi/10.1103/PhysRev.21.143 .
[49] H. Ott, Die Raumgitter der Lithiumhalogenide, Phys. Z. 24 (1923) 209–213.
[50] A. Kirfel, G. Will, R.F. Stewart, The chemical bonding in lithium metaborate, $LiBO_2$. charge densities and electrostatic properties, Acta Cryst. B 39 (2) (1983) 175–185. http://scripts.iucr.org/cgi-bin/paper?a22096 .
[51] H. Effenberger, J. Zemann, Verfeinerung der Kristallstruktur des Lithiumkarbonates, Li_2CO_3*, Z. Kristallogr. 150 (1979) 133–138.
[52] X. Wu, F.R. Fronczek, L.G. Butler, Structure of $LiNO_3$: point charge model and sign of the ^{7}Li quadrupole coupling constant, Inorg. Chem. 33 (7) (1994) 1363–1365.
[53] J. Cabana, C.D. Ling, J. Oró-Solé, D. Gautier, G. Tobías, S. Adams, E. Canadell, M. R. Palacín, Antifluorite-Type lithium chromium oxide nitrides: synthesis, structure, order, and electrochemical properties, Inorg. Chem. 43 (22) (2004) 7050–7060.
[54] J.M. Bijvoet, A. Karssen, X-ray investigation of the crystal structure of lithium oxide, Recl. Trav. Chim. Pays-Bas 43 (10) (1924) 680–684. http://onlinelibrary.wiley.com/doi/10.1002/recl.19240431002/abstract .
[55] L.G. Cota, P.D.L. Mora, On the structure of lithium peroxide Li_2O_2, Acta Cryst. B 61 (2) (2005) 133–136. http://onlinelibrary.wiley.com/doi/10.1107/S0108768105003629/abstract .
[56] H. Dachs, Bestimmung der Lage des Wasserstoffs in LiOH durch Neutronenbeugung, Z. Kristallogr. 112 (1-6) (1959) 60–67. https://www.degruyter.com/view/j/zkri.1959.112.issue-1-6/zkri.1959.112.jg.60/zkri.1959.112.jg.60.xml?format=INT .
[57] E. Perenthaler, H. Schulz, A. Rabenau, Die Strukturen von $LiAlCl_4$ und $NaAlCl_4$ als Funktion der Temperatur, Z. anorg. allg. Chem. 491 (1) (1982) 259–265. http://onlinelibrary.wiley.com/doi/10.1002/zaac.19824910133/abstract .
[58] J. Zemann, Die Kristallstruktur von Lithiumphosphat, Li3PO4, Acta Cryst. 13 (11) (1960) 863–867. http://onlinelibrary.wiley.com/doi/10.1107/S0365110X60002132/abstract .
[59] C. Röhr, R. Kniep, Die Kristallstrukturen von $Li[PF_6]$ und $Li[AsF_6]$, Z. Naturforsch. B 49 (5) (1994) 650–654. https://www.degruyter.com/view/j/znb.1994.49.issue-5/znb-1994-0514/znb-1994-0514.xml .
[60] N.W. Alcock, D.A. Evans, H.D.B. Jenkins, Lithium sulphate – a redetermination, Acta Cryst. B 29 (2) (1973) 360–361. http://onlinelibrary.wiley.com/doi/10.1107/S0567740873002499/abstract .
[61] A. Claassen, The crystal structure of the anhydrous alkali monosulphides. I, Recl. Trav. Chim. Pays-Bas 44 (9) (1925) 790–794. http://onlinelibrary.wiley.com/doi/10.1002/recl.19250440907/abstract .
[62] A. Rosenzweig, B. Morosin, A reinvestigation of the crystal structure of $LiIO_3$, Acta Cryst. 20 (6) (1966) 758–761. http://onlinelibrary.wiley.com/doi/10.1107/S0365110X66001804/abstract .
[63] R.E. Dinnebier, U. Behrens, F. Olbrich, Solid state structures of cyclopentadienyllithium, -sodium, and -potassium. determination by High-Resolution powder diffraction, Organometallics 16 (17) (1997) 3855–3858.
[64] H. Lerner, M. Bolte, An orthorhombic modification of lithium chloride monohydrate, Acta Cryst. E 59 (2) (2003) i20–i21. http://onlinelibrary.wiley.com/doi/10.1107/S1600536803001594/abstract .
[65] K. Hermansson, J.O. Thomas, I. Olovsson, Hydrogen bond studies. CXXXVIII. neutron diffraction studies of $LiNO_3$ $3H_2O$ at 120 and 295 k, Acta Cryst. B 36 (5) (1980) 1032–1040. http://onlinelibrary.wiley.com/doi/10.1107/S0567740880005237/abstract .
[66] K. Hermansson, J.O. Thomas, The experimental electron density in lithium hydroxide monohydrate, Acta Cryst. B 38 (10) (1982) 2555–2563. http://onlinelibrary.wiley.com/doi/10.1107/S0567740882009376/abstract .
[67] J. Lundgren, Å. Kvick, M. Karppinen, R. Liminga, S.C. Abrahams, Neutron diffraction structural study of pyroelectric Li_2SO_4 H_2O at 293, 80, and 20 K, J. Chem. Phys. 80 (1) (1984) 423–430. http://aip.scitation.org/doi/abs/10.1063/1.446465 .
[68] S.J. Clark, M.D. Segall, C.J. Pickard, P.J. Hasnip, M.J. Probert, K. Refson, M.C. Payne, First principles methods using CASTEP, Z. Kristallogr. 220 (5–6) (2005) 567–570. http://discovery.ucl.ac.uk/170173/ .
[69] H. Eckert, Z. Zhang, J.H. Kennedy, Glass formation in non-oxide chalcogenide systems. structural elucidation of Li_2S-SiS_2-LiI solid electrolytes by quantitative ^{29}Si, ^{6}Li and ^{7}Li high resolution solid state NMR methods, J. Non-Cryst. Solids (1989) 271–282.
[70] H. Eckert, Z. Zhang, J.H. Kennedy, Solid state NMR studies of ionically conductive Non-Oxide chalcogenide glasses, Symposium M – Solid State Ionics I, vol. 135, 1988, p. 259. http://journals.cambridge.org/article_S1946427400391953 .
[71] J. Xiao, J. Hu, D. Wang, D. Hu, W. Xu, G.L. Graff, Z. Nie, J. Liu, J. Zhang, Investigation of the rechargeability of Li–O_2 batteries in non-aqueous electrolyte, J. Power Sources 196 (13) (2011) 5674–5678. http://www.sciencedirect.com/science/article/pii/S0378775311004873 .
[72] G. Larraz, A. Orera, J. Sanz, I. Sobrados, V. Diez-Gómez, M.L. Sanjuán, NMR study of Li distribution in $Li_{7-x}H_xLa_3Zr_2O_{12}$ garnets, J. Mater. Chem. A 3 (10) (2015) 5683–5691. http://pubs.rsc.org/en/content/articlelanding/2015/ta/c4ta04570j .
[73] C. Marino, L. Boulet, P. Gaveau, B. Fraisse, L. Monconduit, Nanoconfined phosphorus in mesoporous carbon as an electrode for Li-ion batteries: performance and mechanism, J. Mater. Chem. 22 (42) (2012) 22713–22720. http://pubs.rsc.org/en/content/articlelanding/2012/jm/c2jm34562e .
[74] G. Wu, Z. Xiong, T. Liu, Y. Liu, J. Hu, P. Chen, Y. Feng, A.T.S. Wee, Synthesis and characterization of a new ternary Imide $Li_2Ca(NH)_2$, Inorg. Chem. 46 (2) (2007) 517–521.
[75] J.P. Kartha, D.P. Tunstall, J.T.S. Irvine, An NMR investigation of lithium occupancy of different sites in the oxide superconductor $LiTi_2O_4$ and related compounds, J. Solid State Chem. 152 (2) (2000) 397–402. http://www.sciencedirect.com/science/article/pii/S0022459600986961 .
[76] Y. Dong, F.J. DiSalvo, Reinvestigation of trilithium phosphide, Li_3P, Acta Cryst. E 63 (4) (2007) i97–i98. http://onlinelibrary.wiley.com/doi/10.1107/S1600536807008422/abstract .
[77] B. León, J.I. Corredor, J.L. Tirado, C. Pérez-Vicente, On the mechanism of the electrochemical reaction of tin phosphide with lithium, J. Electrochem. Soc. 153 (10) (2006) A1829–A1834. http://jes.ecsdl.org/content/153/10/A1829 .
[78] X. Wu, S. Wang, X. Lin, G. Zhong, Z. Gong, Y. Yang, Promoting long-term cycling performance of high-voltage Li_2CoPO_4F by the stabilization of

electrode/electrolyte interface, J. Mater. Chem. A 2 (4) (2014) 1006–1013. http://pubs.rsc.org/en/content/articlelanding/2014/ta/c3ta13801a .
[79] R. Mercier, J.P. Malugani, B. Fahys, J. Douglande, G. Robert, Synthese, structure cristalline et analyse vibrationnelle de l'hexathiohypodiphosphate de lithium $Li_4P_2S_6$, J. Solid State Chem. 43 (2) (1982) 151–162. http://www.sciencedirect.com/science/article/pii/0022459682902249 .
[80] B. Key, M. Morcrette, J. Tarascon, C.P. Grey, Pair distribution function analysis and solid state NMR studies of silicon electrodes for lithium ion batteries: Understanding the (De)lithiation mechanisms, J. Am. Chem. Soc. 133 (3) (2011) 503–512.
[81] T.R. Krawietz, D.K. Murray, J.F. Haw, Alkali metal oxides, peroxides, and superoxides: a multinuclear MAS NMR study, J. Phys. Chem. A 102 (45) (1998) 8779–8785.
[82] E. Witt, C.V. Chandran, P. Heitjans, Slow ion exchange in crystalline $Li_2SO_4H_2O$: a ^{6}Li 2D EXSY NMR investigation, Solid State Ion. 304 (2017) 60–64. http://www.sciencedirect.com/science/article/pii/S0167273816309225 .
[83] S. Hayashi, K. Hayamizu, Accurate determination of NMR chemical shifts in alkali halides and their correlation with structural factors, B. Chem. Soc. Jpn. 63 (3) (1990) 913–919. http://www.journal.csj.jp/doi/abs/10.1246/bcsj.63.913 .
[84] E. Weiss, Die Kristallstruktur des Lithiumjodid-Monohydrats, Z. Anorg. Allg. Chem. 341 (3-4) (1965) 203–206. http://onlinelibrary.wiley.com/doi/10.1002/zaac.19653410311/abstract .
[85] A.D. Becke, A new mixing of Hartree–Fock and local density-functional theories, J. Chem. Phys. 98 (2) (1993) 1372–1377. https://aip.scitation.org/doi/10.1063/1.464304 .
[86] J.P. Perdew, M. Ernzerhof, K. Burke, Rationale for mixing exact exchange with density functional approximations, J. Chem. Phys. 105 (22) (1996) 9982–9985. https://aip.scitation.org/doi/10.1063/1.472933 .
[87] A. Tkatchenko, M. Scheffler, Accurate molecular van der waals interactions from Ground-State electron density and Free-Atom reference data, Phys. Rev. Lett. 102 (7) (2009) 073005. https://link.aps.org/doi/10.1103/PhysRevLett.102.073005 .
[88] F. Ortmann, F. Bechstedt, W.G. Schmidt, Semiempirical van der waals correction to the density functional description of solids and molecular structures, Phys. Rev. B 73 (20) (2006) 205101. https://link.aps.org/doi/10.1103/PhysRevB.73.205101 .
[89] S. Grimme, Semiempirical GGA-type density functional constructed with a long-range dispersion correction, J. Comput. Chem. 27 (15) (2006) 1787–1799. https://onlinelibrary.wiley.com/doi/abs/10.1002/jcc.20495 .
[90] P. Jurecka, J. Cerný, P. Hobza, D.R. Salahub, Density functional theory augmented with an empirical dispersion term. Interaction energies and geometries of 80 noncovalent complexes compared with ab initio quantum mechanics calculations, J. Comput. Chem. 28 (2) (2007) 555–569.
[91] M. Vijayakumar, S. Kerisit, K.M. Rosso, S.D. Burton, J.A. Sears, Z. Yang, G.L. Graff, J. Liu, J. Hu, Lithium diffusion in $Li_4Ti_5O_{12}$ at high temperatures, J. Power Sources 196 (4) (2011) 2211–2220. http://www.sciencedirect.com/science/article/pii/S0378775310016666 .
[92] M. Wilkening, D. Gebauer, P. Heitjans, Diffusion parameters in single-crystalline Li_3N as probed by ^{6}Li and ^{7}Li spin-alignment echo NMR spectroscopy in comparison with results from ^{8}Li β-radiation detected NMR, J. Phys.: Condens. Matter 20 (2) (2008) 022201. http://stacks.iop.org/0953-8984/20/i=2/a=022201 .
[93] B. Bader, P. Heitjans, H. Stockmann, H. Ackermann, W. Buttler, P. Freilander, G. Kiese, C. van der Marel, A. Schirmer, Li^+ diffusion in the fast ionic conductor li_3n investigated by beta -radiation detected NMR, J. Phys.: Condens. Matter 4 (20) (1992) 4779. http://stacks.iop.org/0953-8984/4/i=20/a=005.
[94] K. Nishida, T. Asai, S. Kawai, Ionic conductivity and NMR relaxation study on Li_3N single crystal, Solid State Commun. 48 (8) (1983) 701–704. http://www.sciencedirect.com/science/article/pii/0038109883900558 .
[95] T. Lapp, S. Skaarup, A. Hooper, Ionic conductivity of pure and doped Li_3N, Solid State Ion. 11 (2) (1983) 97–103. http://www.sciencedirect.com/science/article/pii/0167273883900450 .
[96] U.v. Alpen, A. Rabenau, G.H. Talat, Ionic conductivity in Li_3N single crystals, Appl. Phys. Lett. 30 (12) (1977) 621–623. http://aip.scitation.org.eaccess.ub.tum.de/doi/abs/10.1063/1.89283 .
[97] R. Messer, H. Birli, K. Differt, NMR study of diffusion in Li_3N, J. Phys. C: Solid State Phys. 14 (20) (1981) 2731. http://stacks.iop.org/0022-3719/14/i=20/a=012 .
[98] K.C. Williams, T.L. Brown, Organometallic exchange reactions. II. Lithium-7 and proton nuclear magnetic resonance spectra of alkyllithium and lithium tetraalkylmetalate solutions in ether, J. Am. Chem. Soc. 88 (18) (1966) 4134–4140, https://doi.org/10.1021/ja00970a004.
[99] H.S. Gutowsky, C.H. Holm, Rate processes and nuclear magnetic resonance spectra. II. Hindered internal rotation of amides, J. Chem. Phys. 25 (6) (1956) 1228–1234. https://aip-scitation-org.eaccess.ub.tum.de/doi/abs/10.1063/1.1743184 .
[100] D. Brinkmann, M. Mali, J. Roos, R. Messer, H. Birli, Diffusion processes in the superionic conductor Li_3N: an NMR study, Phys. Rev. B 26 (9) (1982) 4810–4825. https://link.aps.org/doi/10.1103/PhysRevB.26.4810 .
[101] M. Dalton, D.P. Tunstall, J. Todd, S. Arumugam, P.P. Edwards, A ^{7}Li NMR study of the superconducting spinel $Li_{1+x}Ti_{2-x}O_4$, J. Phys.: Condens. Mat. 6 (42) (1994) 8859. http://iopscience.iop.org.eaccess.ub.tum.de/0953-8984/6/42/016 .
[102] L. Aldon, P. Kubiak, M. Womes, J.C. Jumas, J. Olivier-Fourcade, J.L. Tirado, J.I. Corredor, C.P. Vicente, Chemical and electrochemical Li-Insertion into the $Li_4Ti_5O_{12}$ spinel, Chem. Mater. 16 (26) (2004) 5721–5725.
[103] P. Krtil, J. Dědeček, T. Kostlánová, J. Brus, ^{6}Li MAS NMR study of lithium insertion into hydrothermally prepared Li-Ti-O spinel, Electrochem. Solid-State Lett. 7 (7) (2004) A163. http://esl.ecsdl.org/cgi/doi/10.1149/1.1737710.
[104] T. Kostlánová, J. Dědeček, P. Krtil, The effect of the inner particle structure on the electronic structure of the nano-crystalline Li–Ti–O spinels, Electrochim. Acta 52 (5) (2007) 1847–1856. http://www.sciencedirect.com/science/article/pii/S0013468606008073 .
[105] M. Wagemaker, E.R.H. van Eck, A.P.M. Kentgens, F.M. Mulder, Li-Ion diffusion in the equilibrium nanomorphology of spinel $Li_{4+x}Ti_5O_{12}$, J. Phys. Chem. B 113 (1) (2009) 224–230.
[106] W. Schmidt, P. Bottke, M. Sternad, P. Gollob, V. Hennige, M. Wilkening, Small Change–Great effect: steep increase of Li ion dynamics in $Li_4Ti_5O_{12}$ at the early stages of chemical Li insertion, Chem. Mater. 27 (5) (2015) 1740–1750.
[107] W. Schmidt, M. Wilkening, Discriminating the mobile ions from the immobile ones in $Li_{4+x}Ti_5O_{12}$: ^{6}Li NMR reveals the main Li^+ diffusion pathway and proposes a refined lithiation mechanism, J. Phys. Chem. C 120 (21) (2016) 11372–11381, https://doi.org/10.1021/acs.jpcc.6b02828.
[108] H. Hain, M. Scheuermann, R. Heinzmann, L. Wünsche, H. Hahn, S. Indris, Study of local structure and Li dynamics in $Li_{4+x}Ti_5O_{12}$ ($0 \leq x \leq 5$) using ^{6}Li and ^{7}Li NMR spectroscopy, Solid State Nucl. Magn. Reson. 42 (2012) 9–16. http://www.sciencedirect.com/science/article/pii/S0926204011001214 .
[109] H.H. Heenen, C. Scheurer, K. Reuter, Implications of occupational disorder on ion mobility in $Li_4Ti_5O_{12}$ battery materials, Nano Lett. 17 (6) (2017) 3884–3888.
[110] Jülich Supercomputing Centre, JURECA: general-purpose supercomputer at Jülich Supercomputing Centre, J. Large-Scale Res. Facilities, vol. 2, A62. https://doi.org/10.17815/jlsrf-2-121.